A robust physics-based model framework of the dew point evaporative cooler: from fundamentals to applications

Jie Lin[1,2,3], Muhammad W. Shahzad[4], Jianwei Li[2], Jianyu Long[1,*], Chuan Li[1], Kian Jon Chua[3]

[1] School of Mechanical Engineering, Dongguan University of Technology, Dongguan 523808, China
[2] Department of Engineering Science, University of Oxford, Parks Road, Oxford, OX1 3PJ, United Kingdom
[3] Department of Mechanical Engineering, National University of Singapore, 9 Engineering Drive 1, Singapore 117575, Singapore
[4]Department of Mechanical and Construction Engineering, Northumbria University, Newcastle Upon Tyne NE1 8ST, United Kingdom.

[*]Corresponding Author: longjy@dgut.edu.cn

Abstract

Owing to its great energy efficiency, dew point evaporative cooling is an ideal solution for cooling of electronics, data centers and electric vehicles, where a large amount of sensible heat is generated. To promote the application of dew point evaporative coolers, a common research gap between theoretical and experimental studies is addressed, i.e., how fundamental understanding can be turned into practical applications? In this paper, a coupled scaling and regression analysis is proposed as the key approach to linking the physics-based model to fast data-driven optimization. Accordingly, a complete model framework is developed for the dew point evaporative cooler by establishing a core regression model with its governing dimensionless numbers. The model is integrated with a robust multi-objective optimization algorithm for real applications. Instant predictions of product air temperature and maximum pressure drop can be obtained from the regression model, while it still retains some physical insights into how the cooling performance is affected by the dominant factors. A few optimization studies are carried out to navigate the optimal design and control strategies of the dew point evaporative cooler under assorted ambient conditions. It is noted that the regression model can accurately predict the experimental data of two coolers within ±5.0% maximum discrepancy, and

subsequent optimization suggests improved cooler designs with 30%–60% enhancement in energy efficiency, compared to an existing cooler prototype.

Keywords: dew point evaporative cooling, scaling analysis, regression model, multi-objective optimization, genetic algorithm

Nomenclatures

a	regression coefficient	*Greek symbols*	
A	area, m^2	δ	thickness, mm
c	specific heat at constant pressure, J/(kg·K)	ε	effectiveness
COP	coefficient of performance	μ	dynamic viscosity, Pa·s
d	desirability	π	dimensionless number, maximum latent heat transfer vs. sensible heat transfer
D	diffusion coefficient, m^2/s	ρ	density, kg/m^3
DE	composite desirability	ω	humidity ratio, g/kg dry air
h	specific enthalpy, J/kg	*Subscripts*	
h_{fg}	latent heat evaporation, J/kg	0	reference state
H	nominal channel height, m	a	air
H_t	total channel height, m	d	dry channel
k	thermal conductivity, W/(m·K)	dp	dew point
L	channel length, m	e	evaporation
$\dot{m}$	mass flow rate, kg/s	f	water film
MSE	mean-square error	m	moist air
n	order of polynomial	o	outlet
N	number of channel pairs	p	product air
p	regression coefficient	pl	plate
P	pressure, Pa	s	supply air
Pr	Prandtl number, kinematic viscosity vs. thermal diffusivity	sa	saturation
$\dot{Q}$	cooling capacity, W	v	water vapor

r	flow rate ratio of working air to supply air (working air ratio)	w	wet channel/working air
Re	Reynolds number, inertia force vs. viscous force	x	x-direction
RH	relative humidity, %	y	y-direction
Sc	Schmidt number, kinematic viscosity vs. mass diffusivity	*Abbreviations*	
t	exponent	CFD	computational fluid dynamics
T	temperature, K	COP	coefficient of performance
u	velocity, m/s	DB	dry bulb
$\dot{V}$	volumetric flow rate, m^3/s	HFC	hydrofluorocarbon
w	weight factor	LMTD	log mean temperature difference
W	channel width, m	NSGA	non-dominated sorting genetic algorithm
$\dot{W}$	power consumption, W	NTU	number of transfer units
x	x-coordinate, m	WB	wet bulb
y	y-coordinate, m/objective function		

1 Introduction

Ever since the Paris Agreement took effect in 2016, the entire world has been committed to undertaking actions to combat climate change and mitigate global warming [1]. Electrification, which was deemed as “the greatest engineering achievement of the 20th century” [2], seems to be the key to a decarbonized society. As the use of electricity explosively grows, an increasing demand for sensible cooling or thermal management has inevitably arisen due to unavoidable electrical impedance in electrified systems. Current approaches to sensible cooling are commonly via forced air or liquid flows, where the former is ineffective and the latter requires a complex closed cycle. On the other hand, the conventional vapor compression chiller, which dominates the commercial air conditioning market, has been of great concerns in the past decades, for its high energy consumption and severe greenhouse effect [3]. According to Kigali amendment [4] agreed by more than 170 countries in 2016, 80-85% of hydrofluorocarbons (HFCs) consumption is expected to phase down by 2047, favoring a cooling cycle without chemical refrigerants. Therefore, it is crucial to develop an alternative cooling technology that is simple, efficient and environmentally friendly.

Dew point evaporative cooling, initially appearing as a potential substitute for the mechanical chillers, is capable of providing substantial cooling for hot and dry air at enormous energy efficiency [5]. This has distinguished itself as an ideal option for cooling of electronics, data centers and electric vehicles. It utilizes the intrinsic potential contained in the unsaturated supply air for water evaporation, during which a large amount of sensible heat is absorbed and converted into the latent heat. More importantly, an innovative flow pattern is designed so that the working air stream used to attract moisture is pre-cooled and separated from the main product air stream in dew point evaporative coolers [6]. This allows the supply air to be cooled to below its wet bulb temperature, approaching its dew point temperature.

Recently, numerous studies have been carried out to facilitate a solid understanding of dew point evaporative cooling processes. A dew point evaporative cooler with corrugated air channels achieved a record of about 52.5 coefficient of performance (COP) under an Australian test standard, i.e., supply air at 37.8 °C dry bulb (DB) and 21.1 °C wet bulb (WB) [7]. A counter-cross-flow dew point evaporative cooler made of polystyrene board with nylon-fibers coated on the wet channel surface attained similar cooling performance to a counter-flow cooler, while the size and weight of the cooler could be reduced by around 50% [8]. The dew point cooler could be coupled with a carbon dioxide (CO_2) refrigeration system to reduce the condenser inlet air temperature [9]. The cooler avoided the operation of the refrigeration system at a transcritical state under hot and dry climates and the COP was enhanced by up to 140%. Additionally, a generic indirect evaporative cooler cell for an improved design with multiple point injections of working air into the wet channels was tested [10]. A remarkable COP of the cooler, ranging from 37 to 78, was reported.

Based on the experimental investigations, a few mathematical models were proposed to physically describe the cooling process. The lumped thermal model is the most common model and has been proved to be accurate enough when the air temperature is the sole concern [11]. Later on, in order to find an analytical approach to the cooling effectiveness, modified ε-number of transfer units (NTU) [12] and log mean temperature difference (LMTD) [13] models were proposed, respectively. Furthermore, computational fluid dynamics (CFD) models [14] were formulated to investigate the coupled flow, concentration and temperature fields in the cooler. These models help to provide insights into the fundamental mechanisms of dew point evaporative cooling and thereby the limiting factors of the cooling performance can be determined [15]. However, the physical models often contain a set of differential governing equations, where expensive numerical computations are necessary to resolve the model complexity. Hence, data-driven models were introduced by training available test data or simulation results using neural network [16] and regression analysis [17]. Such models have been tested effective in deriving functional relationships between objective variables and assorted design parameters, without cultivating the relevant physics. Owing to their fast response, data-driven models are exclusively favorable in optimizing the dew point evaporative cooler according to changing demands and constraints [18].

It should be acknowledged that there seems to exist a clear border between physics-based models and data-driven models, hindering cross-disciplinary communications among engineers, physicists and mathematicians. Previous physical models can well explain the dew point evaporative cooling process but are inefficient for optimization and control purposes. Data-driven models, in contrast, are specifically developed to obtain instant estimations of the cooler output, even if large error may occur under extrapolation. Under this circumstance, it is worth arguing if there can be a link between the two different types of models, which has the virtues of both models.

Currently, the answer to the aforementioned scientific issue is not available in the literature. It requires a model that preserves a minimal complexity of physics to reach a fast computing speed, but still elucidates a thorough understanding of relevant physical processes. In this context, scaling analysis would be a potential approach, which provides a perspective of correlating an objective variable with its dominant dimensionless numbers [19].

Therefore, this paper aims to propose a new model framework that can bridge the gap between physics-based models and data-driven models. By unique coupling of scaling analysis, regression analysis and multi-objective optimization, the model demonstrates an ideal integration between in-depth fundamental understanding and fast-response practical applications. The governing dimensionless numbers of the dew point evaporative cooler are identified from an early-established CFD model, each of which captures a specific mechanism that drives the cooling process. A regression analysis is conducted to model an explicit functional relationship between the objective variables and dimensionless numbers. With the governing factors taken into account, the complexity of the regression model can be substantially simplified while it still retains the fundamental understanding of relevant physics. The regression model is incorporated into a multi-objective optimization algorithm for design and control purposes. To summarize, the scope of this work is illustrated in Fig. 1.

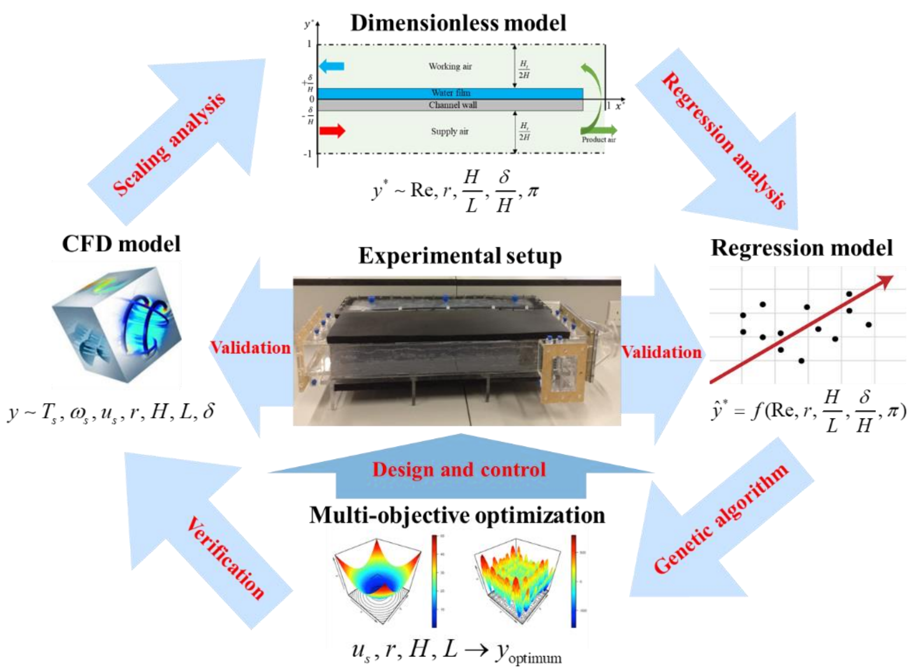

Fig. 1. Scope of the model framework.

2 Mathematical model

The counter-flow dew point evaporative cooler is comprised of multiple channel pairs in stack, as shown in Fig. 2(a), where a channel pair contains a dry and a wet air channel. Theoretically, the cooling process is identical in different channel pairs, which makes it possible to simplify the model geometry from the entire cooler to a generic model domain. As shown in Fig. 2(b), the generic model domain is the smallest unit of a full cooler geometry, consisting of half dry and wet channel pair and a layer of channel wall and water film in between.

Subsequently, a mathematical model is established for the generic model geometry to capture the fundamental dew point evaporative cooling process. A thorough understanding of the cooler's effectiveness and efficiency via the in-depth scaling and regression analyses requires all the relevant physical mechanisms taken into account [20]. This necessitates a CFD model concerning the velocity, temperature and concentration fields of the cooler. Previously, a 2D CFD model with momentum, energy and species balances for laminar flows has been established for the dew point evaporative cooler, where the Reynolds number of the air flows in the cooler is usually below 1500. The model equations are presented in Table 1 [21].

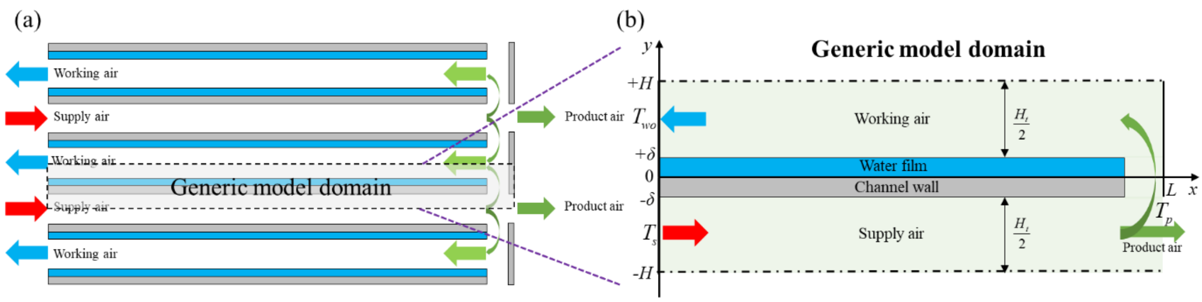

Fig. 2. Modeling of the dew point evaporative cooler: (a) air channel layout; and (b) generic model geometry.

Table 1 CFD model of the dew point evaporative cooler.

Domain	Governing equation	Boundary conditions
Supply air	$\rho_a(\vec{u}_d \cdot \nabla)\vec{u}_d = -\nabla P_d + \mu_m \nabla^2 \vec{u}_d$ (1)	$u_{dx}\big\rvert_{x=0} = u_s, u_{dy}\big\rvert_{x=0 \text{ or } y=-H} = 0$ (2)
	$\nabla \cdot \vec{u}_d = 0$ (3)	$\vec{u}_d\big\rvert_{y=-\delta} = \vec{0}, P_d\big\rvert_{x=L} = 0$ (4)
	$\rho_a c_m \vec{u}_d \cdot \nabla T_d = k_m \nabla^2 T_d$ (5)	$T_d\big\rvert_{x=0} = T_s, \frac{\partial T_d}{\partial x}\big\rvert_{x=L} = 0, \frac{\partial T_d}{\partial y}\big\rvert_{y=-H} = 0$ (6)
Working air	$\rho_a(\vec{u}_w \cdot \nabla)\vec{u}_w = -\nabla P_w + \mu_m \nabla^2 \vec{u}_w$ (7)	$u_{wx}\big\rvert_{x=L} = -ru_s, u_{wy}\big\rvert_{x=L \text{ or } y=H} = 0$ (8)
	$\nabla \cdot \vec{u}_w = 0$ (9)	$\vec{u}_w\big\rvert_{y=\delta} = \vec{0}, P_w\big\rvert_{x=0} = 0$ (10)
	$\rho_a c_m \vec{u}_w \cdot \nabla T_w = k_m \nabla^2 T_w$ (11)	$T_w\big\rvert_{x=L} = T_d, \frac{\partial T_w}{\partial x}\big\rvert_{x=0} = 0, \frac{\partial T_w}{\partial y}\big\rvert_{y=H} = 0$ (12)
		$k_m \frac{\partial T_w}{\partial y}\big\rvert_{y=\delta} + h_{fg} D_{va} \frac{\partial \rho_v}{\partial y}\big\rvert_{y=\delta} = k_f \frac{\partial T_f}{\partial y}\big\rvert_{y=\delta}$ (13)
	$\vec{u}_w \cdot \nabla \rho_v = D_{va} \nabla^2 \rho_v$ (14)	$\rho_v\big\rvert_{x=L} = \rho_{vs}, \rho_v\big\rvert_{y=\delta} = \rho_{v,sa}(T_f)$ (15)
		$\frac{\partial \rho_v}{\partial x}\big\rvert_{x=0} = 0, \frac{\partial \rho_v}{\partial y}\big\rvert_{y=H} = 0$ (16)
Channel plate	$k_{pl} \nabla^2 T_{pl} = 0$ (17)	$\frac{\partial T_{pl}}{\partial x}\big\rvert_{x=0 \text{ or } L} = 0, \frac{\partial T_f}{\partial x}\big\rvert_{x=0 \text{ or } L} = 0$ (18)
Water film	$k_f \nabla^2 T_f = 0$ (19)	$k_m \frac{\partial T_d}{\partial y}\big\rvert_{y=-\delta} = k_{pl} \frac{\partial T_{pl}}{\partial y}\big\rvert_{y=-\delta}$ (20)

In the above model, the dew point evaporative cooling performance can be characterized by the objective variables to be solved, i.e., temperature, humidity, velocity and pressure fields. The relevant physical parameters that have an impact on the cooling performance can be obtained from the governing and boundary equations. These parameters represent the operating and geometric conditions of the cooler, as well as the ambient air conditions, summarized in Table 2.

Table 2 Design and objective variables in the model.

Ambient air conditions	Operating conditions	Geometric conditions	Objective variables
$T_s, \omega_s(\rho_{vs})$	u_s, r	H, L, δ	$T, \omega(\rho_v), \vec{u}, P$

Although the dimensional physical model is able to accurately simulate the cooling process, it does not necessarily reveal the real governing factors that dominate the cooling performance. For example, increasing the channel length may achieve similar cooling effect as does reducing the channel height. Owing to this, using the dimensional model for design and optimization purpose would incur repetitive simulation and verification efforts. Indeed, it is the aspect ratio of the channel (*H*/*L*) that controls the cooling performance. Concurrently, there are other nontrivial ratios that represent different characteristics of the cooler, to be identified. It is therefore more appropriate to optimize the cooler design by evaluating its dominant dimensionless numbers. More importantly, these numbers lay a good foundation for the ensuing regression analysis, allowing a simple and yet accurate cooler model to be obtained.

The key dimensionless numbers to the dew point evaporative cooling process can be derived from a detailed scaling analysis [22]. This is carried out by nondimensionalizing independent and dependent variables so that their magnitude is bounded in the order of 1. Following that, the model equations can be converted into a dimensionless form, and the relevant parameters in the equations will turn into a set of dimensionless numbers. The dimensionless model is provided in Table 3.

Table 3 Dimensionless model of the dew point evaporative cooler.

Independent variables	$x^* = \frac{x}{L}, \quad y^* = \frac{y}{H}, \quad u_x^* = \frac{u_x}{u_s}, \quad u_y^* = \frac{u_y L}{u_s H}$	(21)
Dependent variables	$T^* = \frac{T - T_s}{T_{s,dp} - T_s}, \quad \rho_v^* = \frac{\rho_v - \rho_{vs}}{\rho_{v,sa}(T_{wo}) - \rho_{vs}}, \quad P^* = \frac{P}{\rho_a u_s^2}$	(22)
Dimensionless numbers	$\mathrm{Re} = \frac{\rho_a u_s H}{\mu_m}, \quad \mathrm{Pr} = \frac{\nu_m}{\alpha_m}, \quad \mathrm{Sc} = \frac{\nu_m}{D_{va}}, \quad \pi = \frac{h_{fg} D_{va} \Delta\rho_{sa}}{k_f \Delta T_{dp}}$	(23)

Domain	Governing equation	Boundary condition
Supply air	$u_{dx}^* \frac{\partial u_{dx}^*}{\partial x^*} + u_{dy}^* \frac{\partial u_{dx}^*}{\partial y^*} = -\frac{\partial P_d^*}{\partial x^*} + \frac{1}{\mathrm{Re}} \frac{H}{L} \frac{\partial^2 u_{dx}^*}{\partial x^{*2}} + \frac{1}{\mathrm{Re}} \frac{L}{H} \frac{\partial^2 u_{dx}^*}{\partial y^{*2}}$ (24)	$u_{dx}^* \Big\vert_{x^*=0} = 1,\ u_{dy}^* \Big\vert_{x^*=0 \text{ or } y^*=-1} = 0$ (25)
	$u_{dx}^* \frac{\partial u_{dy}^*}{\partial x^*} + u_{dy}^* \frac{\partial u_{dy}^*}{\partial y^*} = -\frac{L^2}{H^2} \frac{\partial P_d^*}{\partial y^*} + \frac{1}{\mathrm{Re}} \frac{H}{L} \frac{\partial^2 u_{dy}^*}{\partial x^{*2}} + \frac{1}{\mathrm{Re}} \frac{L}{H} \frac{\partial^2 u_{dy}^*}{\partial y^{*2}}$ (26)	$\vec{u}_d^* \Big\vert_{y^*=-\frac{\delta}{H}} = \vec{0}, P_d^* \Big\vert_{x^*=1} = 0$ (27)
	$\frac{\partial u_{dx}^*}{\partial x^*} + \frac{\partial u_{dy}^*}{\partial y^*} = 0$ (28)	
	$\mathrm{Re}\,\mathrm{Pr} \frac{H}{L} u_{dx}^* \frac{\partial T_d^*}{\partial x^*} + \mathrm{Re}\,\mathrm{Pr} \frac{H}{L} u_{dy}^* \frac{\partial T_d^*}{\partial y^*} = \frac{H^2}{L^2} \frac{\partial^2 T_d^*}{\partial x^{*2}} + \frac{\partial^2 T_d^*}{\partial y^{*2}}$ (29)	$T_d^* \Big\vert_{x^*=0} = 0, \frac{\partial T_d^*}{\partial x^*} \Big\vert_{x^*=1} = 0, \frac{\partial T_d^*}{\partial y^*} \Big\vert_{y^*=-1} = 0$ (30)
Working air	$u_{wx}^* \frac{\partial u_{wx}^*}{\partial x^*} + u_{wy}^* \frac{\partial u_{wx}^*}{\partial y^*} = -\frac{\partial P_w^*}{\partial x^*} + \frac{1}{\mathrm{Re}} \frac{H}{L} \frac{\partial^2 u_{wx}^*}{\partial x^{*2}} + \frac{1}{\mathrm{Re}} \frac{L}{H} \frac{\partial^2 u_{wx}^*}{\partial y^{*2}}$ (31)	$u_{wx}^* \Big\vert_{x^*=1} = -r, u_{wy}^* \Big\vert_{x^*=1 \text{ or } y^*=1} = 0$ (32)
	$u_{wx}^* \frac{\partial u_{wy}^*}{\partial x^*} + u_{wy}^* \frac{\partial u_{wy}^*}{\partial y^*} = -\frac{L^2}{H^2} \frac{\partial P_w^*}{\partial y^*} + \frac{1}{\mathrm{Re}} \frac{H}{L} \frac{\partial^2 u_{wy}^*}{\partial x^{*2}} + \frac{1}{\mathrm{Re}} \frac{L}{H} \frac{\partial^2 u_{wy}^*}{\partial y^{*2}}$ (33)	$\vec{u}_w^* \Big\vert_{y^*=\frac{\delta}{H}} = \vec{0},, P_w^* \Big\vert_{x^*=0} = 0$ (34)
	$\frac{\partial u_{wx}^*}{\partial x^*} + \frac{\partial u_{wy}^*}{\partial y^*} = 0$ (35)	
	$\mathrm{Re}\,\mathrm{Pr} \frac{H}{L} u_{wx}^* \frac{\partial T_w^*}{\partial x^*} + \mathrm{Re}\,\mathrm{Pr} \frac{H}{L} u_{wy}^* \frac{\partial T_w^*}{\partial y^*} = \frac{H^2}{L^2} \frac{\partial^2 T_w^*}{\partial x^{*2}} + \frac{\partial^2 T_w^*}{\partial y^{*2}}$ (36)	$T_w^* \Big\vert_{x^*=1} = T_d^*, \frac{\partial T_w^*}{\partial x^*} \Big\vert_{x^*=0} = 0, \frac{\partial T_w^*}{\partial y^*} \Big\vert_{y^*=1} = 0$ (37)
		$\frac{k_m}{k_f} \frac{\partial T_w^*}{\partial y^*} \Big\vert_{y^*=\frac{\delta}{H}} + \pi \frac{\partial \rho_v^*}{\partial y^*} \Big\vert_{y^*=\frac{\delta}{H}} = \frac{\partial T_f^*}{\partial y^*} \Big\vert_{y^*=\frac{\delta}{H}}$ (38)
	$\mathrm{Re}\,\mathrm{Sc} \frac{H}{L} u_{wx}^* \frac{\partial \rho_v^*}{\partial x^*} + \mathrm{Re}\,\mathrm{Sc} \frac{H}{L} u_{wy}^* \frac{\partial \rho_v^*}{\partial y^*} = \frac{H^2}{L^2} \frac{\partial^2 \rho_v^*}{\partial x^{*2}} + \frac{\partial^2 \rho_v^*}{\partial y^{*2}}$ (39)	$\rho_v^* \Big\vert_{x^*=1} = 0, \rho_v^* \Big\vert_{y^*=\frac{\delta}{H}} = \rho_{v,sa}^*(T_f)$ (40)
		$\frac{\partial \rho_v^*}{\partial x^*} \Big\vert_{x^*=0} = 0, \frac{\partial \rho_v^*}{\partial y^*} \Big\vert_{y^*=1} = 0$ (41)

Channel plate	$\frac{H^2}{L^2}\frac{\partial^2 T_{pl}^*}{\partial x^{*2}}+\frac{\partial^2 T_{pl}^*}{\partial y^{*2}}=0$ (42)	$\left.\frac{\partial T_{pl}^*}{\partial x^*}\right\vert_{x^*=0\text{ or }1}=0,\ \left.\frac{\partial T_f^*}{\partial x^*}\right\vert_{x^*=0\text{ or }1}=0$ (43)
Water film	$\frac{H^2}{L^2}\frac{\partial^2 T_f^*}{\partial x^{*2}}+\frac{\partial^2 T_f^*}{\partial y^{*2}}=0$ (44)	$\frac{k_m}{k_{pl}}\left.\frac{\partial T_d^*}{\partial y^*}\right\vert_{y^*=-\frac{\delta}{H}}=\left.\frac{\partial T_{pl}^*}{\partial y^*}\right\vert_{y^*=-\frac{\delta}{H}}$ (45)

In Table 3, $\Delta T_{dp}=T_{s,dp}-T_s$, $\Delta\rho_{sa}=\rho_{v,sa}(T_{wo})-\rho_{vs}$. $\rho_{v,sa}(T_{wo})$ is the theoretical limit of the water vapor density at the working air outlet, calculated at a working air ratio of 0.50 from the following equation

$$\dot{m}_s h(T_s)+\dot{m}_e h_f=\dot{m}_p h(T_{s,dp})+\dot{m}_w h(T_{wo}) \tag{46}$$

Here, $\dot{m}_e=\dot{V}_w(\rho_{v,sa}(T_{wo})-\rho_{vs})$.

The overall performance of the cooler, i.e., the objective variables, is determined by the dimensionless numbers that occur in the dimensionless model [22]. Despite some dimensionless numbers that denote the physical properties of the substances and are not likely to be manipulated, the dependent variables of the model are finally related to the following dimensionless numbers

$$T^*,\omega^*,u_x^*,u_y^*,P^*\sim \mathrm{Re}, r, \frac{H}{L}, \frac{\delta}{H}, \pi \tag{47}$$

In Eqn. (47), the dimensionless numbers represent the critical operating conditions, geometric parameters and ambient conditions that should be considered in the design process (see Table 5).

3 Regression analysis

The regression analysis is a statistical approach to model the functional relationship between a response variable y and multiple predictor variables (regressors) x_1, x_2, …, x_p, denoted as

$$y=f(x_1,x_2,\ldots,x_p) \tag{48}$$

where the function involves a set of unknown regression coefficients (a_1, a_2, …, a_r) to be solved.

In Eqn. (48), there are numerous types of functions and their combinations that can be defined between the response variables and regressors, such as linear, quadratic, exponential, etc [23].

Parameterization of the regression coefficients in the function requires enough observed values of the response variable from a large data set of regressors. The data set is then employed to train the regression coefficients so that the error between observed values and predicted values from the function is minimized.

In this study, a fast regression model of the dew point evaporative cooler is developed, based on its dominant dimensionless numbers. The beauty of investigating the dimensionless numbers is that a simple, stable and accurate functional relationship between the dependent variables and dimensionless numbers can be developed. Unlike the physical parameters which usually requires a machine learning method [24] to implicitly train a complex model, a conventional and yet efficient regression analysis can be applied to the dimensionless numbers [22].

In dew point evaporative cooler, the cooling effectiveness and energy efficiency are of major concerns, and they are associated with product air temperature and pressure drop. In fact, the dimensionless product air temperature is equivalent to the dew point effectiveness of the cooler, expressed as

$$\varepsilon_{dp} = T_p^* = \frac{T_p - T_s}{T_{s,dp} - T_s} \tag{49}$$

On the other hand, the energy efficiency of the cooler (COP), is defined as the ratio of cooling capacity to power consumption in the following equation

$$COP = \frac{\dot{Q}}{\dot{W}} \tag{50}$$

The cooling capacity of the cooler, $\dot{Q}$, is calculated as

$$\dot{Q} = \rho_a \dot{V}_p (h_s - h_p) = \rho_a \dot{V}_p c_m \left(T_s - T_p\right) \tag{51}$$

The theoretical fan power consumption is calculated from the maximum pressure drop of the cooler

$$\dot{W} = \dot{V}_s \Delta P \tag{52}$$

where $\Delta P = P_s - P_{wo}$.

In practice, the fan power consumption under different operating conditions can be estimated via the affinity laws (fan laws) from a known reference state, expressed as below [18]

$$\left(\frac{\dot{W}}{\dot{W}_0}\right) = \left(\frac{\dot{V}_s}{\dot{V}_{s0}}\right)\left(\frac{\Delta P}{\Delta P_0}\right) \tag{53}$$

where $\dot{W}_0$, $\dot{V}_{s0}$ and ΔP_0 are the fan power, air flow rate and pressure drop at the reference state.

Therefore, the dimensionless product air temperature and pressure drop are set to be the two response variables in the regression analysis, with the regressors being the dimensionless numbers in Eqn. (47). Subsequently, a polynomial function is assumed for the regression model, initially written as

$$y = \sum_{i=1}^{r} a_i \, \mathrm{Re}^{p_{1,i}} \, r^{p_{2,i}} \left(\frac{H}{L}\right)^{p_{3,i}} \left(\frac{\delta}{H}\right)^{p_{4,i}} \pi^{p_{5,i}} \tag{54}$$

In Eqn. (54), the regression coefficients are a_i, $p_{1,i}$, $p_{2,i}$, $p_{3,i}$, $p_{4,i}$, $p_{5,i}$, and the exponents of the dimensionless numbers in each term (for any i) must satisfy

$$\sum_{j=1}^{5} p_{j,i} \le n \tag{55}$$

where n is the degree (highest order) of the polynomial function. During regression, it will be adjusted to ensure a reasonable fit that balances the equation simplicity and prediction accuracy.

After the regression model is established, the training data need to be imported to parameterize the model, which is to be acquired via the validated CFD cooler model in Section 2. Similar to the design of experiments, the simulation conditions in the training data set should be carefully determined so that the cooler performance can be effectively observed with only a few data points. This is usually achieved by varying each regressor within its given range to form various combinations of the regressors [25]. Multiple experiment design methods have been proposed to specify the parameter combinations, such as central composite design, random design and full grid design [26]. In this work, a full grid design is used to generate all possible combinations of the parameters, yielding a large number of simulation cases. For each key physical parameter, a wide range is defined and divided into 4 levels in Table 4. This leads to a total of 4^6=4096 cases in the training data set. The values of the corresponding dimensionless numbers (regressors) are provided in Table 5.

Numerical simulations of the CFD cooler model with the total training cases are processed in the COMSOL multiphysics platform, where a finite element method is used to discretize the partial differential equations. More details of the simulation scheme are available in [20].

Table 4 Design of the simulation conditions for regression analysis.

Parameter	Unit	Symbol	Level			
Supply air temperature	°C	T_s	30.0	35.0	40.0	45.0
Supply air humidity	g/kg	ω_s	9.0	12.0	15.0	18.0
Supply air velocity	m/s	u_s	1.0	2.0	3.0	4.0
Working air ratio	–	r	0.2	0.3	0.4	0.5
Channel length	m	L	0.5	1.0	1.5	2.0
Channel height	mm	H_t	2.0	3.0	4.0	5.0

Table 5 Physical representations and ranges of dimensionless numbers

Dimensionless number	Physical representation	Range
Re	Ratio of inertia force to viscous force	68–672
r	Flow rate ratio of working air to supply air	0.2–0.5
$\frac{H}{L}$	Aspect ratio of height to length	0.0006–0.0054

$\dfrac{\delta}{H}$	Aspect ratio of plate thickness to channel thickness	0.07–0.17
π	Ratio of maximum latent heat transfer to sensible heat transfer	0.06–0.08

The observed values of the response variables from the training data set are compared with their predicted values computed via the regression function. In Table 5, it is noticed that the dimensionless numbers have different orders of magnitude, varying from O(0.0001) to O(100). This has caused some difficulties in fitting the regression coefficients. Thus some dimensionless numbers (e.g., Re and $\dfrac{H}{L}$) are multiplied with a factor to adjust their magnitude close to O(1), in the intermediate regression process. Also, it has been found that introducing a logarithm to some dimensionless numbers and an exponent to the response variable can dramatically reduce the required polynomial degree. The final functional relationship for the dimensionless product air temperature and pressure drop are simplified into the forms of

$$T_p^* = \left(\sum_i a_i \,\mathrm{Re}^{p_{1,i}}\, r^{p_{2,i}} \left(\frac{H}{L}\right)^{p_{3,i}} \left(\frac{\delta}{H}\right)^{p_{4,i}} \pi^{p_{5,i}} \right)^{1/t} \quad \text{with } n = 3 \tag{56}$$

$$\Delta P^* = \left(\sum_i a_i (\log \mathrm{Re})^{p_{1,i}}\, r^{p_{2,i}} \left(\log\left(\frac{H}{L} \times 10^3\right) \right)^{p_{3,i}} \left(\frac{\delta}{H}\right)^{p_{4,i}} \pi^{p_{5,i}} \right)^{1/t} \quad \text{with } n = 2 \tag{57}$$

The formulated regression model can be applied to instantly calculate the dimensionless product air temperature and pressure drop within the entire ranges of response variables specified in Table 4 or Table 5.

4 Optimization algorithm

The regression model can be employed to enable the real-time simulation of the cooler performance. When it comes to an optimization process, this translates into dozen times of computation efficiency and time saving, in contrast to thermodynamic models [27]. Therefore, an optimization framework is constructed based on the performed scaling and regression analyses in previous sections. As discussed in Section 3, the dew point effectiveness and COP of the dew point evaporative cooler are given in Eqn. (49) and (50). Additionally, the cooling capacity in Eqn. (51) is essential as a physical measure of the cooling effect delivered by the cooler to a specific application. These three parameters are able to reflect the overall thermodynamic performance of the dew point evaporative cooler. Hence, they are set as the objective variables in the optimization, denoted as

$$y_i \in \left\{ \varepsilon_{dp}, \dot{Q}, \mathrm{COP} \right\} \tag{58}$$

Furthermore, the decision variables to be optimized should be the key physical parameters provided in Table 2 that are adjustable in the design process. Apparently, while the plate and film thickness should be minimized to reduce the transverse thermal resistance, the supply air temperature and humidity are confined to the local climatic conditions. Therefore, the number of decision variables are reduced to

$$x_i \in \left\{ u_s, r, H, L \right\} \tag{59}$$

The lower and upper limits of the decision variables in the optimization are specified in Table 6, which are properly determined from the regression analysis, as well as previous experience in experimental and numerical investigations [28]. The reference point is determined from the existing cooler prototype V2 to be presented in Section 5, which acts as a baseline for optimization.

Table 6 Optimization ranges of the decision variables.

Decision variable	Unit	Symbol	Reference	Lower limit	Upper limit
Channel length	m	L	0.60	0.50	2.00
Channel height	mm	H_t	3.00	2.00	5.00
Supply air velocity	m/s	u_s	2.00	1.00	4.00

Working air ratio	–	r	0.33	0.20	0.50

In addition, a geometric constraint should be applied to the scale of the cooler, to accomplish a fair comparison in terms of cooling performance and fabrication cost. Here, the total surface area of the air channels is confined by

$$L \cdot W \cdot N = A_0 \tag{60}$$

where N is 100, and A_0 is a constant.

Several earlier studies [27, 29, 30] have proposed a multi-objective optimization algorithm that converts multiple objective variables into a single desirability value. In contrast to the non-dominated sorting genetic algorithm (NSGA), optimizing the desirability can achieve appropriate trade-offs among three or more objective variables, while not leading to their inapplicable extreme values. Following this, the multi-to-single-objective optimization method using the genetic algorithm is employed [31]. The desirability function is introduced to normalize each objective variable to order 1, given by its desired value $y_i^{\max}$ and least acceptable value $y_i^{\min}$ [32]

$$d_i = \begin{cases} 1 & \text{for } \hat{y}_i \geq y_i^{\max} \\ \dfrac{y_i^{\max} - \hat{y}_i}{y_i^{\max} - y_i^{\min}} & \text{for } y_i^{\min} < \hat{y}_i < y_i^{\max} \\ 0 & \text{for } \hat{y}_i \leq y_i^{\min} \end{cases} \tag{61}$$

Eventually, the composite desirability combines the contributions made by all objective variables, expressed as below

$$DE = \prod_i d_i^{w_i} \tag{62}$$

where w_i is a user-defined weight factor of y_i and it satisfies $\sum w_i = 1$.

5 Results and discussions

The regression model for the dew point evaporative cooler is first parameterized and validated with CFD simulations and experimental measurements. It is then employed for multi-objective optimization to demonstrate its feasibility in fast-response design and control, which bridges the gap between physics-based and data-driven models.

5.1. Regression model validation

To investigate the practically achievable performance of the dew point evaporative cooler, two dew point evaporative coolers with different physical dimensions have been designed and fabricated, as shown in Fig. 3. The specifications and test conditions of the coolers, together with the consequent dimensionless numbers, are listed in Table 7. Detailed information of the cooler configuration and test system is available in [14, 20]. Resistance temperature detectors (1/10 DIN, Omega Engineering), air velocity meters (±2.0% full scale, Omega Engineering), differential pressure sensors (±1.0% full scale, Omega Engineering) and multimeter (Keysight) were employed for temperature, flow rate, pressure and power measurements. The acquired test results act as a good stepping stone to validate the proposed regression model and optimize the cooler design.

(a) (b)

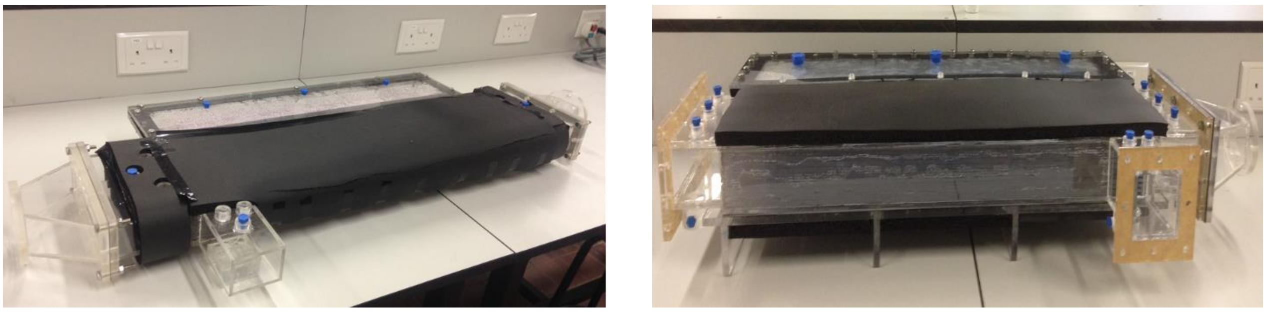

Fig. 3. Prototypes of dew point evaporative coolers: (a) prototype V1; and (b) prototype V2.

Table 7 Test conditions of the dew point evaporative cooler.

Parameter	Unit	Prototype V1		Prototype V2	
		Nominal value	Range	Nominal value	Range
Channel length	m	0.6	–	0.6	–
Channel height	mm	5.0	–	3.0	–
Number of channel pairs	–	5	–	10	–
Supply air temperature	°C	30.0	30.0–35.0	35.0	30.0–40.0
Supply air humidity	g/kg	16.5	12.0–18.0	11.0	10.5–12.0
Supply air velocity	m/s	1.50	0.9–2.2	2.00	1.0–2.0
Working air ratio	–	0.50	0.20–0.50	0.33	0.20–0.50
Re	–	256	153–375	211	106–211
$\frac{H}{L}$	–	0.0046	–	0.0029	–
$\frac{\delta}{H}$	–	0.09	–	0.14	–
π	–	0.071	0.066–0.074	0.070	0.068–0.071

Following Eqn. (56) and (57), the correlations for dimensionless product air temperature and pressure drop were parameterized with a minimum complexity that was ever found to achieve an acceptable maximum error, i.e., within ±10.0%. The ultimate coefficients of the regression model are provided in Appendix A. Fig. 4 shows the regression errors of the model in fitting the training data set with reference to the CFD model, where the regression error is defined as

$$\text{Regression error} = \frac{\hat{y}_i - y_i}{y_i} \times 100\% \tag{63}$$

It is observed that the maximum regression errors of dimensionless product air temperature and pressure drop are within ±10.0% and ±7.0%, respectively. The mean square errors (MSEs) of the two response variables are found to be 1.91×10^{-4} and 0.94, and their coefficient of determination (R^2) are above 0.99, indicating a nearly perfect fit of each response variable.

(a) (b)

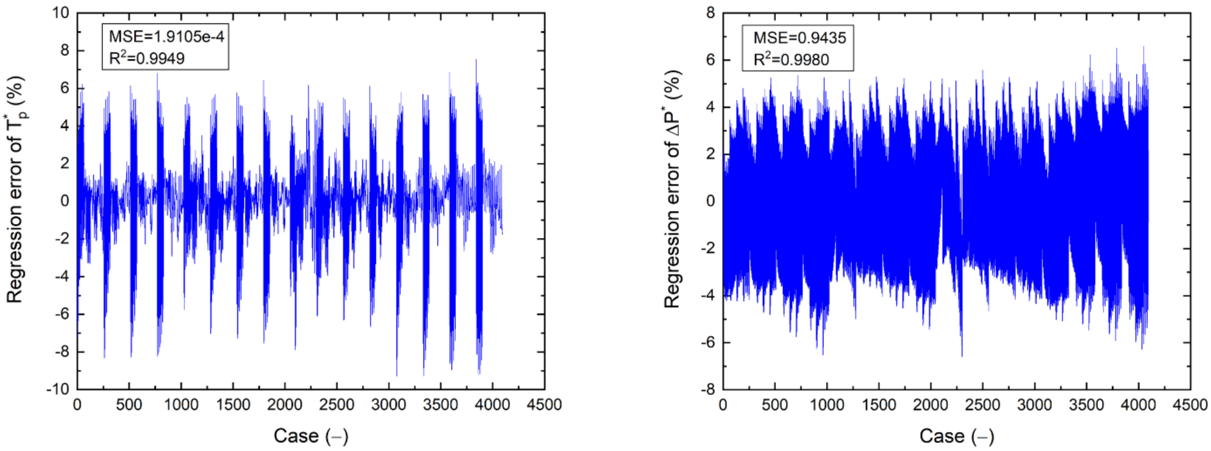

Fig. 4. Regression errors of: (a) dimensionless product air temperature; and (b) dimensionless pressure drop.

The feasibility of the proposed regression model is further examined before it is incorporated into the optimization framework. By reproducing the test conditions of prototype V1 and V2, the model is validated with the experimental results. As shown in Fig. 5(a) and (b), the maximum pressure drops calculated from Eqn. (57) is compared with test data of prototype V2 at different supply air velocities and working air ratios, spanning 1.0–2.0 m/s and 0.20–0.50, respectively. The supply air conditions were at their nominal values listed in Table 7, i.e., 35.0 °C and 11.0 g/kg. The error bars of the data points indicate the experimental uncertainty [14]. It is clear that the regression model can predict the pressure drop of the cooler mostly within its experimental uncertainty, although it consistently underestimates the flow resistance. The maximum discrepancy between the predicted values and observed values is about ±5.0%. Similarly, model validation of product air temperature at different operating conditions is presented in Fig. 5(c) and (d). The correlated function achieves good agreement with both prototypes, and the maximum discrepancy remains within ±2.4%. Besides, validation of the product air temperature is carried out at varying supply air temperature and humidity, and the regression model stays highly reliable.

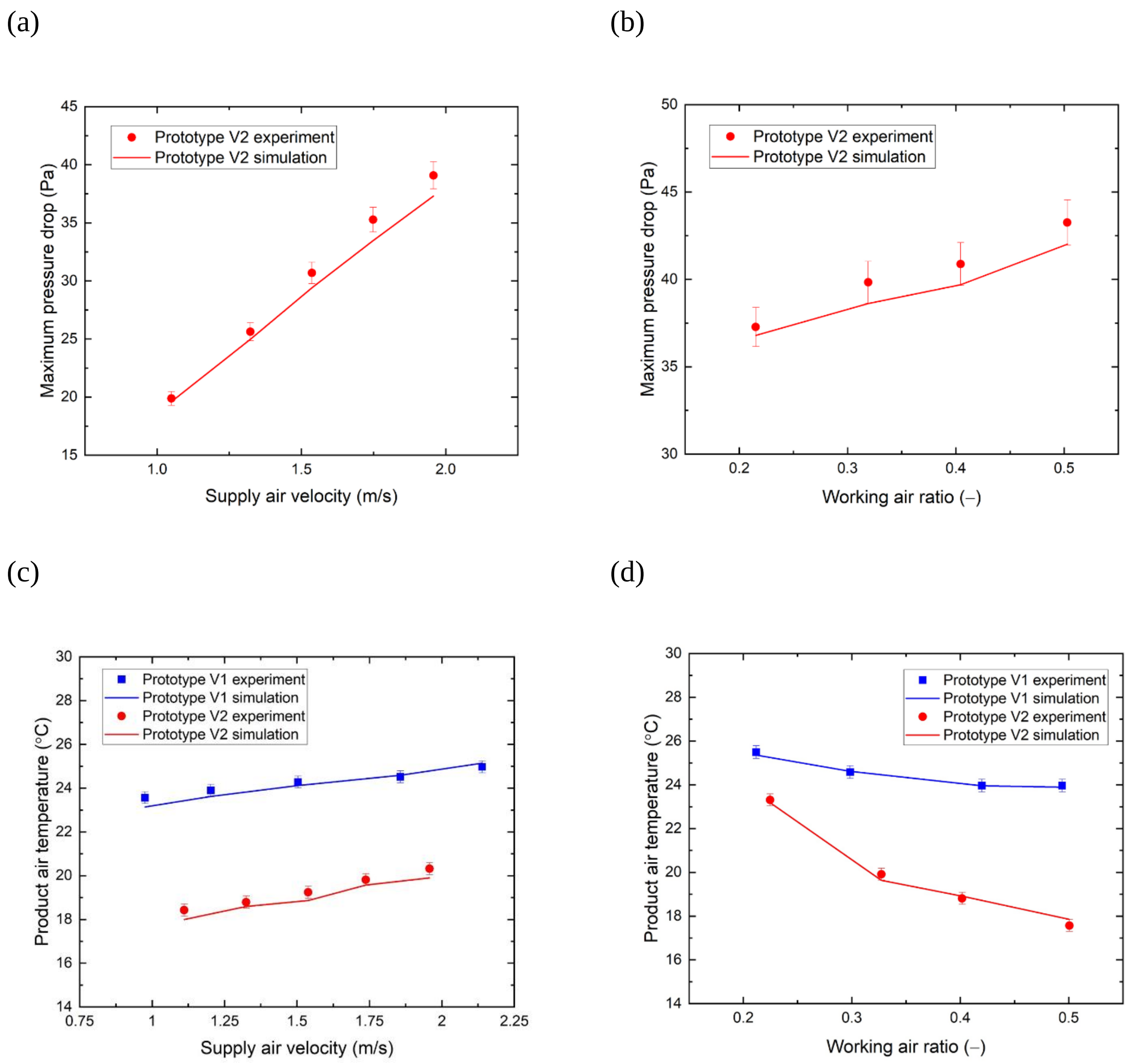

Fig. 5. Model validation with test results of prototype V1 and V2: (a) maximum pressure drop vs. supply air velocity; (b) maximum pressure drop vs. working air ratio; (c) product air temperature vs. supply air velocity; and (d) product air temperature vs. working air ratio.

5.2. Preference-based optimization

Subsequently, the regression model is integrated into the multi-to-single-objective optimization with genetic algorithm. In this optimization, the weight factors in the composite desirability can be varied to emphasize different preferences of the three objective variables, i.e., dew point effectiveness, cooling capacity and COP. Concurrently, the least accepted value and desired value should be appropriately selected for the desirability function of each objective variable, according to their practical achievable ranges.

To demonstrate the capability of the proposed model framework, identical conditions to an earlier study [27] are defined in the present preference-based optimization. The optimization is conducted under two supply air conditions and four preference scenarios, and the necessary parameters are given in Table 8.

Table 8 Parameters of the desirability function in multi-to-single-objective optimization [27].

Parameter		Dew point effectiveness	Cooling capacity	COP
		–	W	–
Weight factor	Equal preference	1/3	1/3	1/3
	ε_{dp}-preference	1/2	1/4	1/4
	$\dot{Q}$- preference	1/4	1/2	1/4
	COP-preference	1/4	1/4	1/2
T_s=30.0 °C	Least accepted value	0.6	1500	10
ω_s=13.3 g/kg	Desired value	0.9	3000	30
T_s=38.0 °C	Least accepted value	0.6	3000	30
ω_s=8.2 g/kg	Desired value	0.9	5000	50

The optimal solutions of the decision variables generated from both regression and CFD models are provided in Table 9. The objective variables and composite desirability of the regression model solutions are re-calculated by the CFD model which acts as a standard.

Apparently, the optimal decision variables suggested by the regression model under different scenarios are close to those from the CFD model. Most of them appear to be even better, in terms of the composite desirability (DE). This reveals that the regression model derived from the scaling analysis owns the merits of great simplicity, fast response and competitive accuracy for simulation and optimization.

On the other hand, it is advised that the channel length be maintained at the minimum available value of 0.5 m and the working air ratio be at 0.40, respectively, with the only exception being ε_{dp}-preference case under 38.0 °C and 8.2 g/kg ambient air conditions. Owing to this, building a cooler with long enough air channels to reach a high cooling effectiveness may not be a wise choice. From a thermodynamic point of view, the channel length has a significant effect on the pressure drop and COP, a shorter length is thus preferred with increasing number of channels, which also delivers more cooling capacity. Furthermore, the loss in dew point effectiveness can be compensated by adjusting the channel height and supply air velocity. Indeed, the channel height and supply air velocity are the two key design parameters that need to be carefully considered according to real situations. The ideal ranges for the channel height and supply air velocity are 3.0–4.0 mm and 1.0–2.0 m/s, respectively, as a result of the trade-offs among the objective variables. This finding is in agreement with most existing prototypes [33-35].

Table 9 Optimal solutions under different preference scenarios.

Supply air	Study	Preference	Decision variables				Objective variables			
			L	H_t	u_s	r	ε_{dp}	$\dot{Q}$	COP	DE
			m	mm	m/s	–	–	W	–	–

30.0 °C 13.3 g/kg 50.0% RH	Present work	Reference	0.60	3.00	2.00	0.33	0.79	2181	17.5	0.4721
		Equal	0.50	3.46	1.60	0.40	0.81	2206	30.0	0.6857
		ε_{dp}	0.50	3.19	1.47	0.40	0.86	1999	30.0	0.7099
		$\dot{Q}$	0.50	3.70	1.72	0.40	0.75	2370	29.5	0.6393
		COP	0.50	3.53	1.63	0.40	0.79	2252	30.0	0.7513
	CFD model [27]	Equal	0.50	3.42	1.58	0.40	0.82	2181	30.1	0.6858
		ε_{dp}	0.50	3.26	1.49	0.40	0.85	2045	30.4	0.7076
		$\dot{Q}$	0.50	3.70	1.75	0.40	0.75	2404	28.9	0.6379
		COP	0.50	3.81	1.61	0.40	0.76	2299	33.6	0.7231
38.0 °C 8.2 g/kg 20.0% RH	Present work	Reference	0.60	3.00	2.00	0.33	0.71	4433	36.8	0.4447
		Equal	0.50	3.15	1.76	0.40	0.76	4690	50.1	0.7607
		ε_{dp}	0.50	3.04	1.60	0.45	0.82	4072	50.0	0.7320
		$\dot{Q}$	0.50	3.28	1.83	0.40	0.73	4896	50.0	0.7922
		COP	0.50	3.12	1.74	0.40	0.76	4620	50.1	0.8153
	CFD model [27]	Equal	0.50	3.15	1.76	0.40	0.76	4690	50.1	0.7607
		ε_{dp}	0.50	2.90	1.61	0.40	0.81	4201	50.0	0.7276
		$\dot{Q}$	0.50	3.40	1.85	0.40	0.72	5018	51.8	0.7846
		COP	0.50	3.22	1.75	0.40	0.75	4719	52.0	0.8077

5.3. Optimization under different ambient conditions

After the regression model and its corresponding optimization algorithm are proved to be effective and efficient, it is expected that the optimization framework could be employed to practical applications. One important goal could be to customize the cooler design according to a specific climate for optimal performance. In this section, the decision variables of the cooler are optimized under varying supply air temperature (30.0–40.0 °C) or humidity (10.0–18.0 g/kg). The weight factors of the objective variables are set equal in the composite desirability, and their least accepted value and desired value are defined as the minimum and maximum values from Section 6.2, as listed in Table 10.

Table 10 Parameters of the desirability function.

Parameter	Dew point effectiveness –	Cooling capacity W	COP –
Weight factor	1/3	1/3	1/3
Least accepted value	0.6	1500	10
Desired value	0.9	5000	50

The optimization results are summarized in Table 11. Obviously, the channel length is constantly at 0.50 m, and the working air ratio only deviates from 0.40 at high supply air humidity. As the supply air humidity raises, the product air temperature is moving towards its thermodynamic limit of dew point temperature. Hence, the working air ratio can be reduced with enlarged channel height to obtain better cooling capacity and COP, whilst the dew point effectiveness does not deteriorate. On the contrary, as the supply air temperature increases, the cooling capacity and consequent COP tend to rise due to larger temperature drops. It is then suggested that the channel height be reduced to ensure a good heat and mass transfer (cooling effectiveness) in the channels, and the supply air velocity should slightly increase to deliver larger cooling capacity. Finally, the dew point effectiveness and COP could be optimized to approach their desired values, while the cooling capacity is highly dependent of the evaporative cooling potential of the supply air. In addition, in line with the results from Table 9, the stability of the optimal channel length under different conditions eliminates the necessity to optimize its value.

Table 11 Optimal design solutions under different ambient conditions.

Supply air temperature	Supply air humidity	Relative humidity	Decision variables				Objective variables			
T_s °C	ω_s g/kg	RH %	L m	H_t mm	u_s m/s	r –	ε_{dp} –	$\dot{Q}$ W	COP –	DE –
30.0	12.0	45.2	0.50	3.77	1.29	0.40	0.80	2180	49.9	0.5033
32.5		39.2	0.50	3.55	1.39	0.40	0.81	2665	49.9	0.6186
35.0		34.1	0.50	3.29	1.44	0.40	0.84	3054	50.0	0.7122
37.5		29.7	0.50	3.16	1.53	0.40	0.85	3554	49.9	0.7903
40.0		26.0	0.50	3.12	1.65	0.40	0.85	4181	50.1	0.8578
35.0	10.0	28.5	0.50	3.09	1.46	0.40	0.83	3295	50.0	0.7335
	12.0	34.1	0.50	3.29	1.44	0.40	0.84	3054	50.0	0.7122
	14.0	39.7	0.50	3.59	1.45	0.40	0.83	2882	49.9	0.6741
	16.0	45.2	0.50	3.66	1.41	0.37	0.85	2545	47.2	0.6173
	18.0	50.7	0.50	3.90	1.38	0.35	0.85	2281	46.4	0.5526

In addition to the design process of the dew point evaporative cooler, it is worth investigating how the operational parameters can be controlled under changing ambient air conditions. Accordingly, the decision variables are reduced to two parameters, namely, supply air velocity and working air ratio. The channel length and height are decided to be 0.50 m and 3.29 mm, which are the optimal solutions from the default supply air conditions (35.0 °C and 12.0 g/kg) in Table 11.

Similarly, the optimal solutions of the operational parameters are listed in Table 12. Although the control parameters do not lead to better composite desirability, in comparison with Table 11, none of the three optimal objective variables (ε_{dp}, $\dot{Q}$, COP) can be entirely dominated by previous solutions.

Hence, it can be inferred that the two sets of optimal solutions stay in the same Pareto-optimal front [36].

Additionally, it should be highlighted that the optimal working air ratio is fixed at 0.40, irrespective of the supply air temperature. The variation of working air ratio under different supply air humidity is in a small range of 0.30–0.45. This partially alleviates the burden of developing a sensitive control strategy to adjust the working air ratio during operations. Therefore, the dew point evaporative coolers can be operated with a relatively simple control system where the supply air velocity or flow rate is required to regulate.

Table 12 Optimal control solutions under different ambient conditions.

Supply air temperature	Supply air humidity	Relative humidity	Decision variables		Objective variables			
T_s	ω_s	RH	u_s	r	ε_{dp}	$\dot{Q}$	COP	DE
°C	g/kg	%	m/s	–	–	W	–	–
30.0	12.0	45.2	1.33	0.40	0.85	2091	39.8	0.4715
32.5		39.2	1.31	0.40	0.86	2456	48.5	0.6095
35.0		34.1	1.44	0.40	0.84	3054	50.0	0.7122
37.5		29.7	1.59	0.40	0.83	3734	50.3	0.7859
40.0		26.0	1.69	0.40	0.82	4371	52.2	0.8441
35.0	10.0	28.5	1.51	0.43	0.81	3377	50.0	0.7259
	12.0	34.1	1.44	0.40	0.84	3054	50.0	0.7122
	14.0	39.7	1.37	0.40	0.88	2645	47.6	0.6618
	16.0	45.2	1.28	0.35	0.88	2310	49.2	0.5732
	18.0	50.7	1.39	0.34	0.88	2200	39.6	0.5144

5.4. Summary

In general, the proposed physical-based optimization framework of the cooler is able to make a judicious choice of design/control parameters to reach a perfect balance of the three objective variables, according to their desirability functions. To clarify this point, the performance improvement of the objective variables with optimal design/control parameters under different ambient conditions is illustrated in Fig. 6, with the baseline at the reference state (L=0.60 m, H_t=3.00 mm, u_s=2.00 m/s and r=0.33) from Table 6 or Table 9.

It is apparent that the COP of the dew point evaporative cooler can be massively enhanced by 30–60%, which is extremely favored to save energy consumption and operational cost. A maximum of

11% improvement for the dew point effectiveness is observed, due to its limited potential in approaching its thermodynamic limit. This translates into a better ability to generate a cooler environment. In contrast, the cooling capacity is moderately sacrificed by up to 18%. However, the cooling capacity of the optimized solutions still ranges from 2.0 to 4.4 kW, which is equivalent to a typical split air conditioner and can be increased by stacking more air channels [37].

In addition, the proposed optimization framework aims to explore the global optimum of the design/control space, where the genetic algorithm is deemed preponderant. Nonetheless, other simple optimization algorithms can also be applied if the design/control space is narrowed or a local optimum is considered sufficient, to further reduce computational power.

(a)

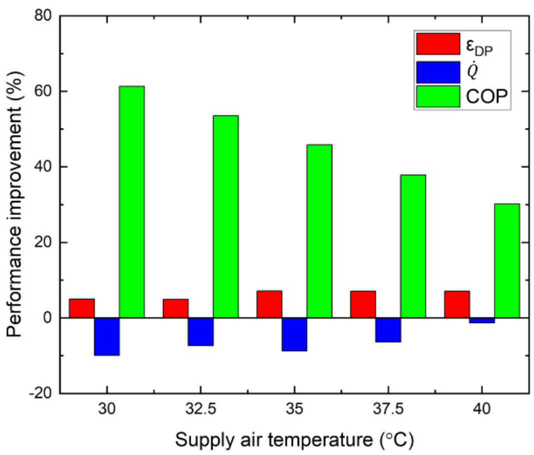

(b)

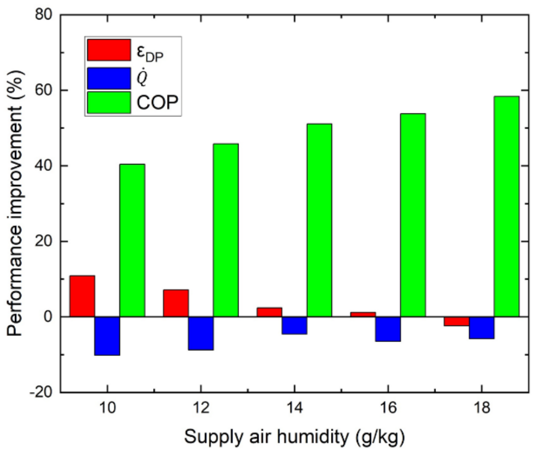

(c)

(d)

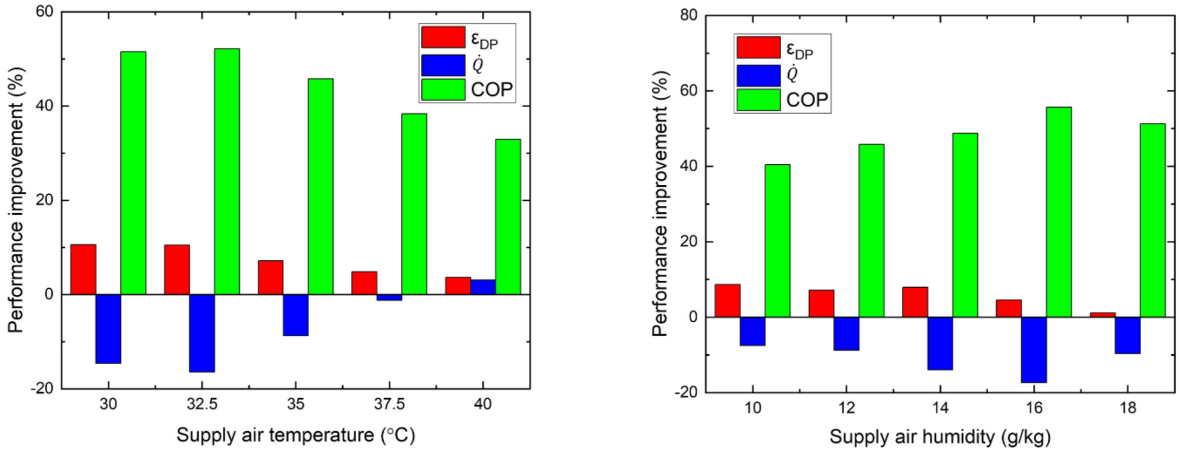

Fig. 6. Performance improvement of objective variables: (a) optimal design parameters at varying T_s; (b) optimal design parameters at varying $_s$; (c) optimal control parameters at varying T_s; and (d) optimal control parameters at varying.

6 Conclusion

A robust physics-based model framework for the dew point evaporative cooler has been proposed in this paper, based on a regression model and an optimization algorithm with its dominant dimensionless numbers. The dimensionless numbers were derived from a proper scaling analysis of an early-established CFD model. With this approach, the complexity of the regression model can be dramatically reduced with good stability and accuracy, compared to conventional regression or machining learning methods using superficial physical parameters. The model can achieve instant predictions of product air temperature and maximum pressure drop within ±5.0% discrepancy. Afterwards, the regression model is integrated with a multi-objective optimization algorithm for cooler design and control.

Subsequent optimization study suggests that the channel length should be consistently designed at its minimum value of 0.50 m, and the working ratio be relatively stable at 0.40. The channel height and supply air velocity are varied in small ranges of 3.0–3.9 mm and 1.2–1.7 m/s, respectively.

Accordingly, the COP and dew point effectiveness of the cooler can be improved by up to 60% and 11%, respectively, at a maximum sacrifice of 18% cooling capacity.

The above results indicate that the design and control space of the dew point evaporative cooler are subjected to a very small degree of freedom, justifying that a simple optimization strategy would be sufficient. Therefore, instead of adopting the complicated genetic algorithm that promotes global optimization at a compromise of computational power, other handy methods can be further employed to enable a real-time optimization.

In addition, the perspective of coupling scaling and regression analyses to achieve cross-scale understanding and applications can be successfully expanded to many research areas.

Appendix A. Regression coefficients

The regression coefficients for the dimensionless product air temperature and maximum pressure drop are presented in Table A1 and A2, respectively.

Table A1 Regression coefficients for dimensionless product air temperature.

i	a	p_1	p_2	p_3	p_4	p_5	i	a	p_1	p_2	p_3	p_4	p_5
1	-0.284	0	0	0	0	0	22	-0.705	0	2	0	1	0
2	22.097	0	0	0	0	1	23	71.872	0	2	1	0	0
3	-99.048	0	0	0	0	2	24	1.550	0	3	0	0	0
4	9.352e-2	0	0	0	1	0	25	2.789e-4	1	0	0	0	0
5	-1.473	0	0	0	1	1	26	-2.552e-3	1	0	0	0	1
6	-7.045e-2	0	0	0	2	0	27	-7.006e-5	1	0	0	1	0
7	53.509	0	0	1	0	0	28	-6.320e-2	1	0	1	0	0
8	-5.178e2	0	0	1	0	1	29	0.117	1	0	1	1	0
9	-14.483	0	0	1	1	0	30	3.421	1	0	2	0	0

10	-4.152e2	0	0	2	0	0	31	-1.427e-3	1	1	0	0	0
11	-5.045e3	0	0	2	1	0	32	1.344e-2	1	1	0	0	1
12	-1.839e4	0	0	3	0	0	33	6.977e-4	1	1	0	1	0
13	2.639	0	1	0	0	0	34	-2.936e-2	1	1	1	0	0
14	-19.437	0	1	0	0	1	35	5.404e-4	1	2	0	0	0
15	0.267	0	1	0	1	0	36	2.164e-7	2	0	0	0	0
16	-1.753e2	0	1	1	0	0	37	-2.464e-6	2	0	0	0	1
17	1.551e3	0	1	1	0	1	38	-5.381e-7	2	0	0	1	0
18	66.504	0	1	1	1	0	39	2.428e-5	2	0	1	0	0
19	9.051e2	0	1	2	0	0	40	2.827e-8	2	1	0	0	0
20	-2.854	0	2	0	0	0	41	-4.509e-11	3	0	0	0	0
21	6.682	0	2	0	0	1							
t	0.1												

Table A2 Regression coefficients for dimensionless pressure drop.

i	a	p_1	p_2	p_3	p_4	p_5	i	a	p_1	p_2	p_3	p_4	p_5
1	2.120	0	0	0	0	0	9	-6.491e-3	0	1	1	0	0
2	0.302	0	0	0	0	1	10	4.356e-2	0	2	0	0	0
3	0.402	0	0	0	1	0	11	-4.321e-1	1	0	0	0	0
4	-4.586e-1	0	0	1	0	0	12	-1.943e-1	1	0	0	0	1
5	4.421e-2	0	0	2	0	0	13	-5.591e-2	1	0	0	1	0
6	-8.946e-2	0	1	0	0	0	14	7.300e-2	1	0	1	0	0
7	1.846	0	1	0	0	1	15	-4.141e-3	1	1	0	0	0
8	1.755e-2	0	1	0	1	0	16	3.549e-2	2	0	0	0	0

t	0.095

Acknowledgement

The authors gratefully acknowledge the generous funding from (1) the Postdoctoral Science Foundation of China Funding Scheme (2019M653379); (2) the National Natural Science Foundation of China Funding Scheme (71801046 and 51775112); and (3) Guangdong Research Foundation (2019B1515120095).

References

[1] The Paris Agreement. United Nations Framework Convention on Climate Change.
[2] G. Constable, B. Somerville. A century of innovation: Twenty engineering achievements that transformed our lives. Joseph Henry Press2003.
[3] A. Handbook. ASHRAE handbook-Fundamentals. ASHRAE, Atlanta, GA, 2013.
[4] E.A. Heath. Amendment to the Montreal protocol on substances that deplete the ozone layer (Kigali amendment). International Legal Materials. 56 (2017) 193-205.
[5] K.J. Chua, S.K. Chou, W.M. Yang, J. Yan. Achieving better energy-efficient air conditioning – A review of technologies and strategies. Appl Energ. 104 (2013) 87-104.
[6] P. Glanville, A. Kozlov, V. Maisotsenko. Dew Point Evaporative Cooling: Technology Review and Fundamentals. ASHRAE Transactions. 117 (2011).
[7] P. Xu, X. Ma, X. Zhao, K. Fancey. Experimental investigation of a super performance dew point air cooler. Appl Energ. 203 (2017) 761-77.
[8] L. Jia, J. Liu, C. Wang, X. Cao, Z. Zhang. Study of the thermal performance of a novel dew point evaporative cooler. Appl Therm Eng. 160 (2019).
[9] M. Belusko, R. Liddle, A. Alemu, E. Halawa, F. Bruno. Performance Evaluation of a CO2 Refrigeration System Enhanced with a Dew Point Cooler. Energies. 12 (2019).
[10] M.W. Shahzad, M. Burhan, D. Ybyraiymkul, S.J. Oh, K.C. Ng. An improved indirect evaporative cooler experimental investigation. Appl Energ. 256 (2019).
[11] B. Riangvilaikul, S. Kumar. Numerical study of a novel dew point evaporative cooling system. Energ Buildings. 42 (2010) 2241-50.
[12] S. Anisimov, D. Pandelidis. Numerical study of the Maisotsenko cycle heat and mass exchanger. Int J Heat Mass Tran. 75 (2014) 75-96.
[13] X. Cui, K.J. Chua, M.R. Islam, W.M. Yang. Fundamental formulation of a modified LMTD method to study indirect evaporative heat exchangers. Energ Convers Manage. 88 (2014) 372-81.
[14] J. Lin, D.T. Bui, R. Wang, K.J. Chua. The counter-flow dew point evaporative cooler: Analyzing its transient and steady-state behavior. Appl Therm Eng. 143 (2018) 34-47.
[15] J. Lin, D.T. Bui, R. Wang, K.J. Chua. On the fundamental heat and mass transfer analysis of the counter-flow dew point evaporative cooler. Appl Energ. 217 (2018) 126-42.
[16] A. Sohani, H. Sayyaadi, S. Hoseinpoori. Modeling and multi-objective optimization of an M-cycle cross-flow indirect evaporative cooler using the GMDH type neural network. International Journal of Refrigeration. 69 (2016) 186-204.

[17] A. Pakari, S. Ghani. Regression models for performance prediction of counter flow dew point evaporative cooling systems. Energ Convers Manage. 185 (2019) 562-73.
[18] A. Sohani, H. Sayyaadi, M. Zeraatpisheh. Optimization strategy by a general approach to enhance improving potential of dew-point evaporative coolers. Energ Convers Manage. 188 (2019) 177-213.
[19] J. Lin, S.-M. Huang, R. Wang, K. Jon Chua. On the in-depth scaling and dimensional analysis of a cross-flow membrane liquid desiccant dehumidifier. Appl Energ. 250 (2019) 786-800.
[20] J. Lin, R.Z. Wang, M. Kumja, T.D. Bui, K.J. Chua. Multivariate scaling and dimensional analysis of the counter-flow dew point evaporative cooler. Energ Convers Manage. 150 (2017) 172-87.
[21] J. Lin, D.T. Bui, R. Wang, K.J. Chua. On the exergy analysis of the counter-flow dew point evaporative cooler. Energy. 165 (2018) 958-71.
[22] W.B. Krantz. Scaling analysis in modeling transport and reaction processes: a systematic approach to model building and the art of approximation. John Wiley & Sons2007.
[23] S. Chatterjee, J.S. Simonoff. Handbook of regression analysis. John Wiley & Sons2013.
[24] G. Zhu, T.-T. Chow, C.K. Lee. Performance analysis of counter-flow regenerative heat and mass exchanger for indirect evaporative cooling based on data-driven model. Energ Buildings. 155 (2017) 503-12.
[25] R. Myers, D. Montgomery. Experiments with mixtures. In response Surface Methodology, Process and Product optimization Using Designed Experiments. New York: Wiley Interscience1995.
[26] T. Lorenzen, V. Anderson. Design of experiments: a no-name approach. CRC Press1993.
[27] J. Lin, R. Wang, C. Li, S. Wang, J. Long, K.J. Chua. Towards a thermodynamically favorable dew point evaporative cooler via optimization. Energ Convers Manage. 203 (2020).
[28] J. Lin, R.Z. Wang, M. Kumja, T.D. Bui, K.J. Chua. Modelling and experimental investigation of the cross-flow dew point evaporative cooler with and without dehumidification. Appl Therm Eng. 121 (2017) 1-13.
[29] Q. Chen, M.K. Ja, Y. Li, K.J. Chua. Energy, economic and environmental (3E) analysis and multi-objective optimization of a spray-assisted low-temperature desalination system. Energy. 151 (2018) 387-401.
[30] S. Anisimov, D. Pandelidis, J. Danielewicz. Numerical study and optimization of the combined indirect evaporative air cooler for air-conditioning systems. Energy. 80 (2015) 452-64.
[31] K. Deb. Multi-objective optimization using evolutionary algorithms. John Wiley & Sons2001.
[32] T.P. Ryan. Modern Experimental Design. Wiley2006.
[33] Z. Duan. Investigation of a novel dew point indirect evaporative air conditioning system for buildings. University of Nottingham2011.
[34] B. Riangvilaikul, S. Kumar. An experimental study of a novel dew point evaporative cooling system. Energ Buildings. 42 (2010) 637-44.
[35] S.T. Hsu, Z. Lavan, W.M. Worek. Optimization of wet-surface heat exchangers. Energy. 14 (1989) 757-70.
[36] J. Long, Z. Sun, P.M. Pardalos, Y. Hong, S. Zhang, C. Li. A hybrid multi-objective genetic local search algorithm for the prize-collecting vehicle routing problem. Inform Sciences. 478 (2019) 40-61.
[37] A. Handbook. ASHRAE Handbook-HVAC Applications. ASHRAE, Atlanta, GA, 2011.